Osmotically driven pipe flows and their relation to sugar transport in plants

KÅRE H. JENSEN[1,2], EMMANUELLE RIO[1,3], RASMUS HANSEN[1], CHRISTOPHE CLANET[4] AND TOMAS BOHR[1]†

[1]Center for Fluid Dynamics, Department of Physics, Technical University of Denmark, Building 309, 2800 Kgs. Lyngby, Denmark

[2]Center for Fluid Dynamics, Department of Micro- and Nanotechnology, Technical University of Denmark, DTU Nanotech Building 345 East, 2800 Kgs. Lyngby, Denmark

[3]Laboratoire de Physique des Solides, Univ. Paris-Sud, CNRS, UMR 8502, F-91405 Orsay Cedex, France

[4]IRPHE, Universités d'Aix-Marseille, 49 Rue Frédéric Joliot-Curie BP 146, F-13384 Marseille Cedex 13, France

In plants, osmotically driven flows are believed to be responsible for translocation of sugar in the pipe-like phloem cell network, spanning the entire length of the plant – the so-called Münch mechanism. In this paper, we present an experimental and theoretical study of transient osmotically driven flows through pipes with semi-permeable walls. Our aim is to understand the dynamics and structure of a 'sugar front', i.e. the transport and decay of a sudden loading of sugar in a water-filled pipe which is closed in both ends. In the limit of low axial resistance (valid in our experiments as well as in many cases in plants) we show that the equations of motion for the sugar concentration and the water velocity can be solved exactly by the method of characteristics, yielding the entire flow and concentration profile along the tube. The concentration front decays exponentially in agreement with the results of Eschrich, Evert & Young (*Planta* (*Berl.*), vol. 107, 1972, p. 279). In the opposite case of very narrow channels, we obtain an asymptotic solution for intermediate times showing a decay of the front velocity as $M^{-1/3}t^{-2/3}$ with time t and dimensionless number $M \sim \eta \kappa L^2 r^{-3}$ for tubes of length L, radius r, permeability κ and fluid viscosity η. The experiments (which are in the small M regime) are in good quantitative agreement with the theory. The applicability of our results to plants is discussed and it is shown that it is probable that the Münch mechanism can account only for the short distance transport of sugar in plants.

1. Introduction

The translocation of sugar in plants, which takes place in the phloem sieve tubes, is not well understood on the quantitative level. The current belief, called the pressure-flow hypothesis (Nobel 1999), is based on the pioneering work of Ernst Münch in the 1920s (Münch 1930). It states, that the motion in the phloem is purely passive, due to the osmotic pressures that build up relative to the neighbouring xylem in response to

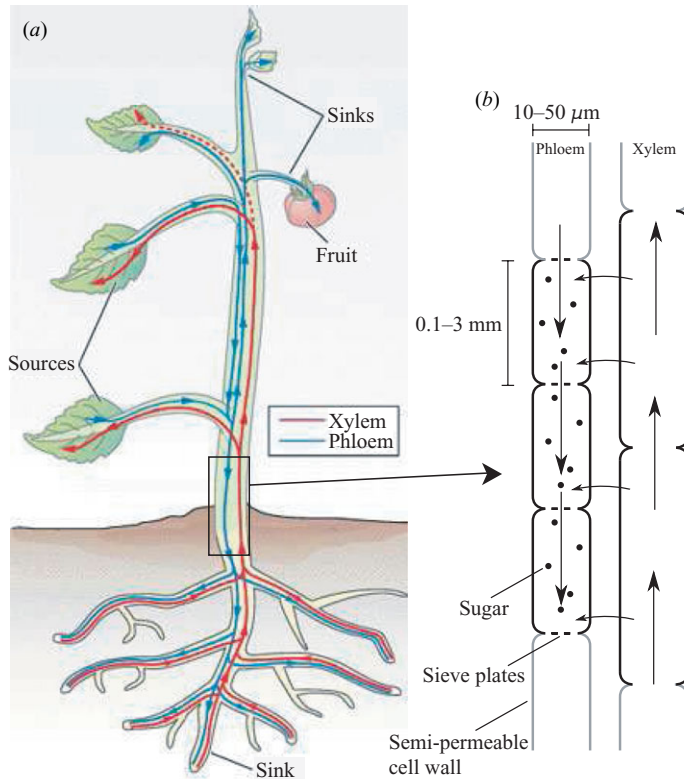† Email address for correspondence: tbohr@fysik.dtu.dk

FIGURE 1. In plants, two separate pipe-like systems are responsible for the transport of water and sugar. The xylem conducts water from the roots to the shoot while the phloem conducts sugar and other nutrients from places of production to places of growth and storage. The mechanism believed to be responsible for sugar translocation in the phloem, called the Münch mechanism or the pressure-flow hypothesis (Nobel 1999), states the following: As sugar is produced via photosynthesis in sources it is actively loaded into the tubular phloem cells. As it enters the phloem, the chemical potential of the water inside is lowered compared to the surrounding tissue, thereby creating a net flux of water into the phloem cells. This influx of water in turn creates a bulk flow of sugar and water towards the sugar sink shown in (b), where active unloading takes place. As the sugar is removed, the chemical potential of the water inside the phloem is raised resulting in a flow of water out of the sieve element.

loading and unloading of sugar in different parts of the plant, as shown in figure 1. This mechanism is much more effective than diffusion, since the osmotic pressure differences caused by different sugar concentrations in the phloem create a bulk flow directed from large concentrations to small concentrations, in accordance with the basic need of the plant. Such flows are often called osmotically driven pressure flows (Thompson & Holbrook 2003), or osmotically driven volume flows (Eschrich, Evert & Young 1972).

To study the osmotically driven flows, Eschrich *et al.* (1972) conducted simple model experiments. Their set-up consisted of a semi-permeable membrane tube submerged in a water reservoir, modelling a phloem sieve element and the surrounding water-filled tissue. At one end of the tube a solution of sugar, water and dye was introduced to mimic the sudden loading of sugar into a phloem sieve element. In the case of the closed tube, they found that the sugar front velocity decayed exponentially in

time as it approached the far end of the tube. Also, they found the initial velocity of the sugar front to be proportional to concentration of the sugar solution. Through simple conservation arguments, they showed that for a flow driven according to the pressure-flow hypothesis, the velocity of the sugar front is given by

$$u_f = \frac{L}{t_0} \exp\left(-\frac{t}{t_0}\right) \quad \text{where} \quad t_0 = \frac{r}{2\kappa\Pi}, \tag{1.1}$$

where t is time, L is the length of the sieve element and r its radius, κ is the permeability of the membrane and Π is the osmotic pressure of the sugar solution. For dilute solutions, $\Pi \approx RTc$ (Landau & Lifshitz 1980), where R is the gas constant, T the absolute temperature and c the concentration in moles per volume. The conservation argument for (1.1) is the following: for incompressible flow in a wide rigid semi-permeable tube of length L imbedded in water, we imagine part of the tube initially filled with sugar solution and the rest with pure water. For a wide tube with slow flow, viscous effects and thus the pressure gradient along the tube is negligible and the pressure is simply equal to the osmotic pressure Π averaged over the tube, i.e. $RT\bar{c}$ where $\bar{c}$ is the constant average sugar concentration. The water (volume) flux through the part of the tube ahead of the sugar front x_f (where there is no osmosis) is $-2\pi r\kappa RT\bar{c}(L - x_f)$, where κ is the permeability of the tube and the flow is negative since water flows out. This will be equal to the rate of change of volume ahead of x_f and thus, due to incompressibility, is equal to $-\pi r^2 dx_f/dt$. Putting these two expressions together we get

$$\frac{\mathrm{d}x_f}{\mathrm{d}t} = \frac{2L_p RT\bar{c}}{r}(L - x_f) = \frac{1}{t_0}(L - x_f) \tag{1.2}$$

leading to $u_f = \mathrm{d}x_f/\mathrm{d}t$ given by (1.1).

In the experiments performed by Eschrich *et al.* (1972) good qualitative agreement with (1.1) was obtained, but on the quantitative level the agreement was rather poor. We thus chose to perform independent experiments along the same lines. Eschrich *et al.* (1972) used dye to track the sugar, and in one of our set-ups we can check this method by directly following the sugar without using dye. Also, we make independent measurements of the membrane properties, which then allow detailed comparison with the predictions showing good quantitative agreement.

Simultaneously with the experiments, we develop the theory for osmotic flows. The above derivation of the front propagation is simplified by the lack of viscosity and diffusion and, indeed, by the very assumption that a well-defined sugar front exists. To go beyond this we must use the coupled equations for the velocity and concentration fields as they vary along the tubes and in time. Here we follow the footsteps of a large number of authors, as discussed later. Our main contribution is the analysis of the decay of an initially localized sugar concentration in a channel closed in both ends described by (4.9) and (4.10). Here we point out that the main dimensionless number (termed as *Münch number*) can be chosen as

$$M = \frac{16\eta L^2 \kappa}{r^3}, \tag{1.3}$$

where η is the fluid viscosity. We show how to simplify the equations and obtain exact solutions in the regimes $M \ll 1$ (the regime of the experiments in this paper and of those of Eschrich *et al.*) and asymptotic solutions for $M \gg 1$. Both regimes are found in plants and we propose an effective way for numerical integration of the equations in the general case using Green's functions. In the regime $M \ll 1$ the solubility of the

Quantity	Magnitude	Reference
Radius (μm)	4.5 (Fava bean), 4 (Winter squash), 6–25	Knoblauch & van Bel (1998), Taiz & Zeiger (2002), Nobel (1999)
Length (mm)	0.09 (Fava bean), 0.1–3	Knoblauch & van Bel (1998), Nobel (1999)
Flow velocity (m h^{-1})	0.5–1, 0.2–2	Knoblauch & van Bel (1998), Nobel (1999)
Elastic modulus (MPa)	17, 5.6–7.4 (Ash)	Thompson & Holbrook (2003a), Niklas (1992)
Permeability (10^{-11} m s^{-1} Pa^{-1})	5,1.1 (Zitella translucence)	Thompson & Holbrook (2003a), Eschrich et al. (1972)
Sucrose concentration (M)]	0.3–0.9	Taiz & Zeiger (2002)

TABLE 1. Characteristic properties of phloem sieve elements.

equations is shown by mapping them to a damped Burgers equation (5.6), which can be solved by the method of characteristics. An analogous relation was pointed out earlier by Frisch (1976), but for a different boundary condition (open in one end) where the damping term disappears. Some results for $M \ll 1$ were also given by Weir (1981), but the lack of generality of his approach to the time-dependent problem makes his results hard to extend.

In table 1 we show characteristic data for single sieve elements, which build up the phloem conducts in plants. If one naively applies these results to the flow inside such sieve elements, taking $L = 1$ mm, $r = 10$ μm, $\kappa = 10^{-11}$ m s^{-1} Pa^{-1} and concentration $\bar{c} = 0.5$ M, one gets a characteristic velocity from (1.1) of 9 m h^{-1}, almost an order of magnitude larger than the range of velocities given in the table. Here one has to remember that the characteristic velocity from (1.1) is valid for a *transient* flow caused by an initial sudden sugar loading, whereas the velocities quoted in the table are characteristic for the normal steady-state operation of the plants. For large distances (e.g. those occurring in tall trees), the viscous effects embodied in (1.3) become large. Thus the value of M for the single sieve element considered above is $M \approx 1.6 \times 10^{-4}$ whereas the value for a phloem tube spanning a distance of 10 m would be greater by a factor 10^8, i.e. $M \approx 1.6 \times 10^4$ (see also table 3 for characteristic values for M). In this regime (1.1) is no longer valid and, in fact, as seen in §5.2 (5.46), the characteristic velocity will be reduced by a factor $M^{-1/3}$, now making it an order of magnitude *smaller* than the velocities quoted in the table. This seems to indicate that large distance transport in trees cannot rely solely on the Münch mechanism and indeed the sieve elements are living cells and active transport may play a key role (see, e.g. Taiz & Zeiger 2002). For future studies in this direction it is important to be able to separate these effects clearly and thus to understand the passive osmotic component as clearly and simply as possible, which is the aim of the present paper.

The layout of the paper is as follows: §§2 and 3 describe our experimental set-ups and the experimental results obtained. In §4, the flow equations are developed and in §5 we present solutions for the cases $M \ll 1$ and $M \gg 1$. Finally, §6 contains a detailed comparison between theory and experiments. After the conclusions (§7), two appendices follow. Appendix A provides information about the experimental materials used and appendix B discusses the numerical methods (based on Green's functions) used for solving the flow equations in the general case.
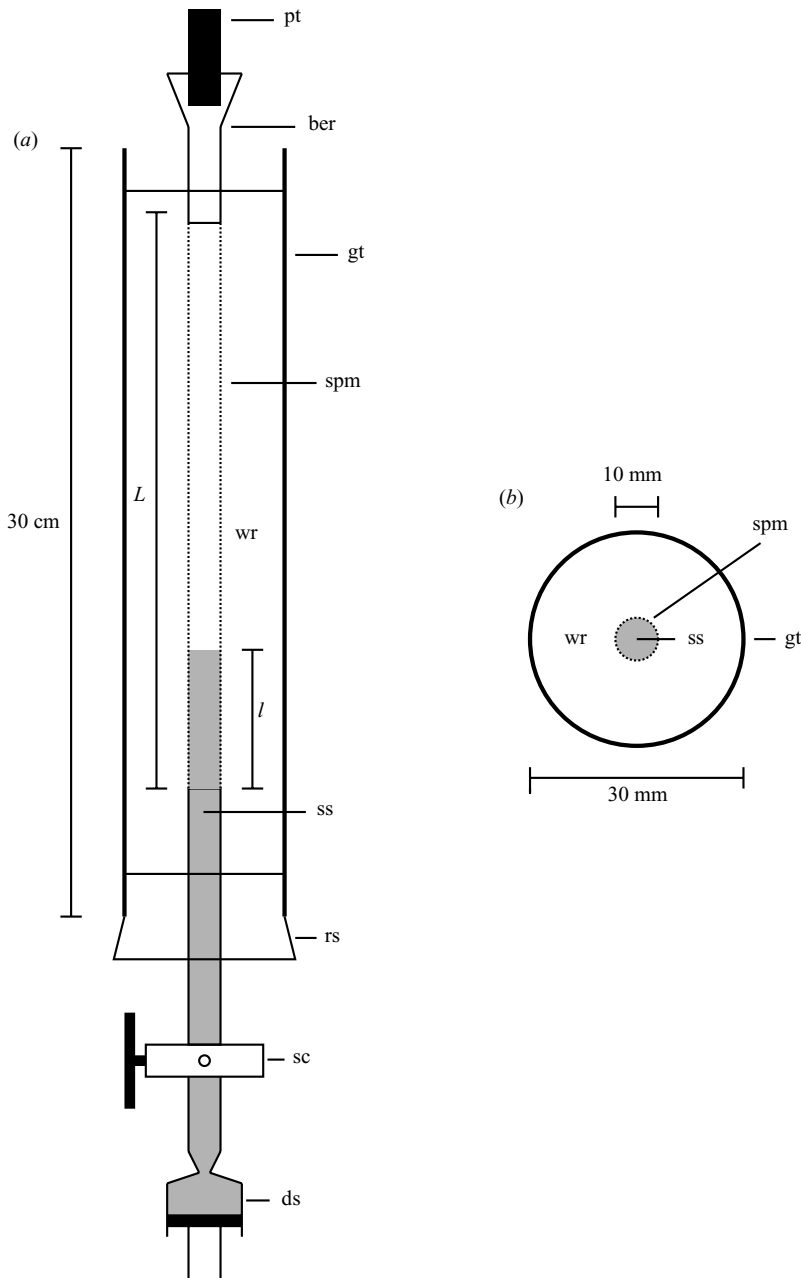
FIGURE 2. Set-up I used to observe the movement of a sugar–dye solution (ss) inside a semi-permeable membrane tube (spm). *L*: length of membrane tube; *l*: initial sugar front height; ds: disposable syringe; gt: glass tube; rs: rubber stopper; sc: stopcock; wr: water reservoir; bc: brass cylinder; pt: pressure transducer.

2. First experimental set-up

2.1. *Set-up and methods*

Set-up I is presented in figure 2. It is based on the design by Eschrich *et al.* with the addition of a pressure transducer that allows us to measure the gauge pressure

	1	2	3	4	5
Mean sugar concentration, $\bar{c}$ (mM)	1.5 ± 0.3	2.10 ± 0.03	2.4 ± 0.2	4.2 ± 0.7	6.8 ± 0.1
Osmotic pressure, Π (bar)	0.14 ± 0.02	0.15 ± 0.01	0.31 ± 0.03	0.39 ± 0.01	0.68 ± 0.02
Membrane tube length, L (cm)	28.5	20.8	28.5	28.5	20.6
Initial front height, l (cm)	4.9	3.7	6.6	6.5	4.8

TABLE 2. Data for the experimental runs shown in figure 3.

(which is what we from now on will refer to as 'pressure') inside the membrane tube continuously. More precisely, it consisted of a 30 cm long, 30 mm wide glass tube in which a semi-permeable membrane tube of equal length and a diameter of 10 mm was inserted. At one end, the membrane tube was fitted over a glass stopcock equipped with a rubber stopper. On the other end, the membrane tube was fitted over a brass cylinder equipped with a holder to accommodate a pressure transducer for measuring the pressure inside the membrane tube.

After filling the 30 mm wide glass tube with water, water was pressed into the semi-permeable tube with a syringe. Care was taken so that no air bubbles were stuck inside the tube. For introducing the sugar solution into the tube, a syringe was filled with the solution and then attached to the lower end of the stopcock which was kept closed. After fitting the syringe, the stopcock was opened and the syringe piston was very slowly pressed in, until a suitable part of the tube had been filled with the solution. Care was also taken to avoid any mixing between the sugar solution and the water already present in the semi-permeable tube. The physical characteristics of the membranes and of the sugar we used are discussed in appendix A. To track the movement of the sugar solution it was mixed with a red dye and data was recorded by taking pictures of the membrane tube at intervals of 15 min using a digital camera.

2.2. Experimental results obtained with set-up I

An example of a set of data is shown in figure 3. In figure 3(*a*) are the raw images, which after processing give figure 3(*b*) showing the position of the sugar front, x_f, as a function of time. The error bars on x_f are estimated to be ± 1 mm, but are too small to be seen. Finally, figure 3(*c*) shows the pressure inside the tube as a function of time. At first, a linear motion of the front is observed with a front velocity of ~ 1 cm h^{-1}. This is then followed by a decrease in the front velocity as the front approaches the end of the tube. The pressure is seen to rise rapidly during the first hour before settling to a constant value, indicated by the dashed line. This constant value is taken to be the osmotic pressure Π of the sugar solution. Looking at figure 3(*a*), one observes that diffusion has the effect of dispersing the front slightly as time passes. Below the front, the concentration seems to be uniform throughout the cross-section of the tube, and there is no indication of large boundary layers forming near the membrane walls.

Similar experiments with different sugar concentrations were made and a plot of the results can be seen in figure 3(*d,e*). The experimental conditions for the five different sets of experiments are given in table 2. Qualitatively the motion of the front and the pressure increase follows the same pattern. One notices that the speed with which the fronts move is related to the mean sugar concentration inside the membrane tube, with the high-concentration solutions moving faster than the low-concentration ones.
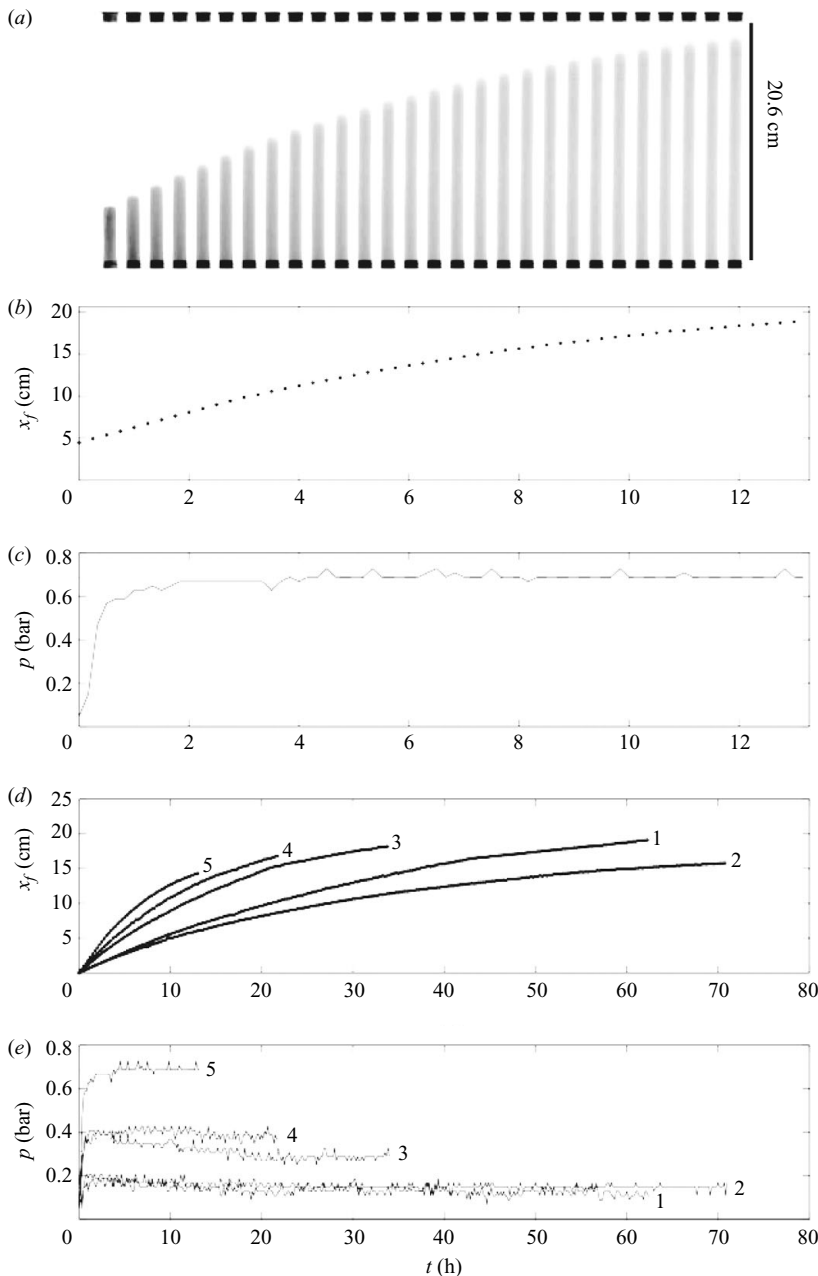
FIGURE 3. Experimental results from set-up I. (*a*) Time series of pictures taken in experiment 5. Time increases from left to right in steps of 30 min. See details of the sugar solutions used in table 2. (*b*) Plot of the front position versus time obtained from the images above. (*c*) Plot of the gauge pressure inside the tube versus time. The dashed line is the osmotic pressure of the solution, taken to be the average value of the pressure from $t = 2$ h until the end of the experiment. (*d*) Plots of the sugar front position versus time for different sugar concentrations, as indicated in table 2. (*e*) Plots of the pressure inside the membrane tube for different sugar concentrations.
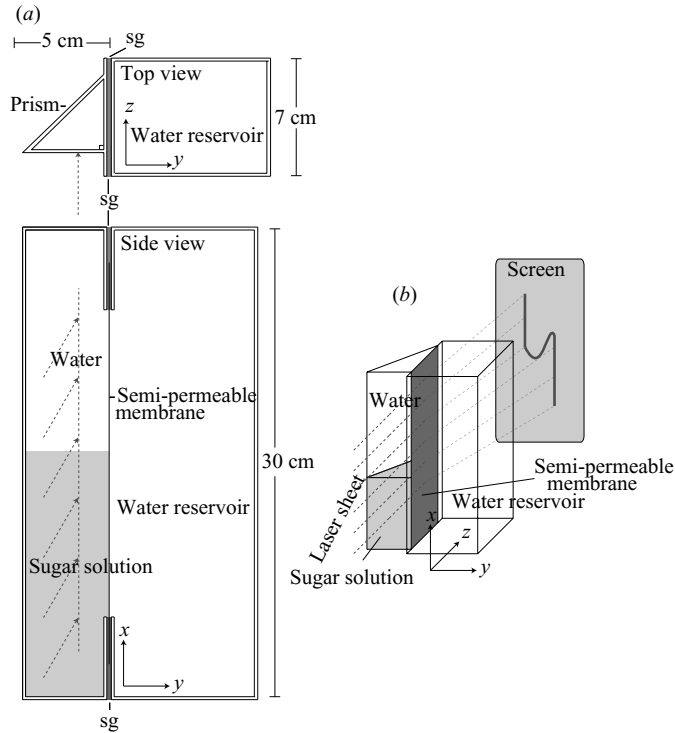
FIGURE 4. Set-up II dedicated to the tracking of the sugar front via index of refraction changes. It consists of a hollow isosceles glass prism and a Plexiglas cuboid in osmotic contact through a membrane. A pressure transducer was attached to the top of the glass prism to measure the pressure inside.

The reason why 2 is moving slower than 1 is that experiment 2 was conducted in a slightly shorter membrane tube than the one used in experiment 1, thereby decreasing the characteristic velocity as we shall see later.

3. Second experimental set-up

3.1. *Set-up and methods*

Set-up II is presented in figure 4. This set-up allows us to track the real front location, without the use of colorant, directly via the variation of the index of refraction. It consisted of a hollow isosceles glass prism and a Plexiglas cuboid in osmotic contact through a membrane. To track the time evolution of the sugar front inside the prism, we used the refraction of a laser sheet passing through it. The laser sheet was generated by shining a laser beam, generated by a Melles Griot 3.1 mW laser, through a glass rod. When passing through the prism, light would deviate depending on the local index of refraction, producing a typical S shape as shown in figure 4. The index of refraction varies linearly with sugar concentration and thus by looking at the refracted laser sheet projected onto a screen, we were able to reconstruct the concentration profile inside the prism. A camera recorded images of the screen at regular intervals to track the moving concentration profile.
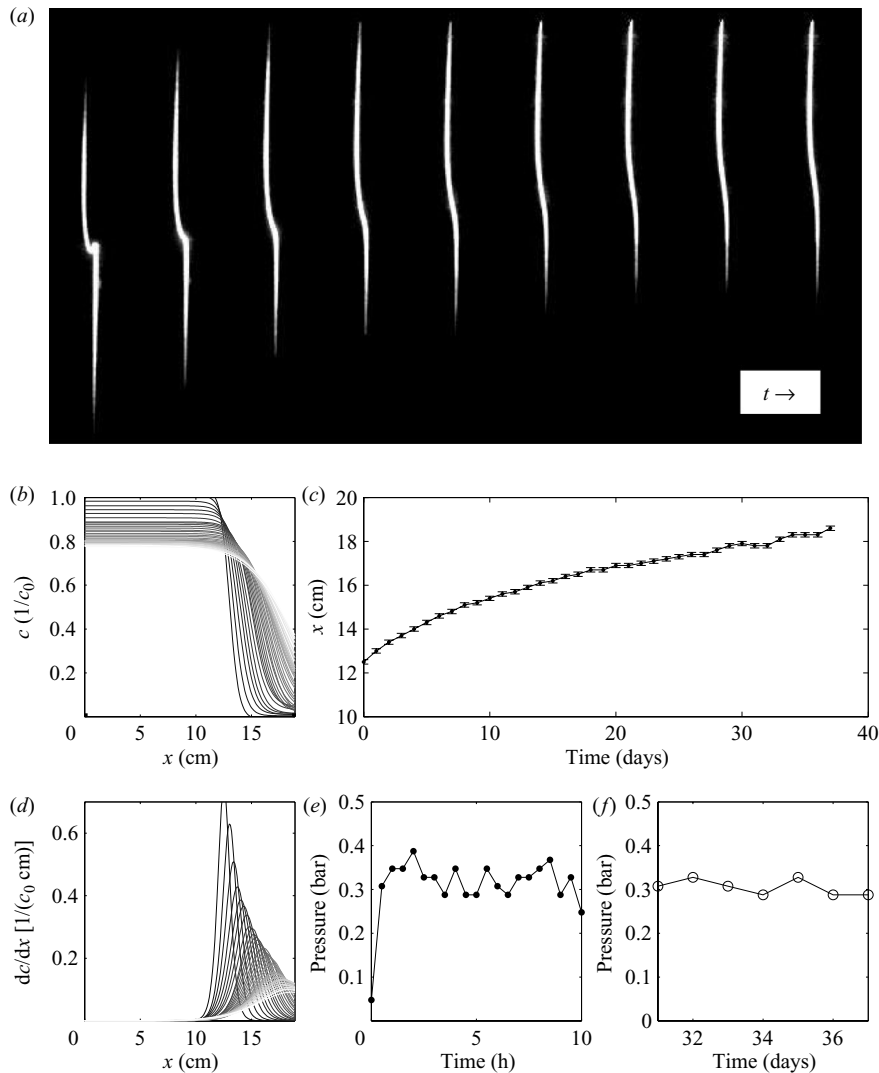
FIGURE 5. Results from set-up II. In (*a*) the raw data images are shown. In (*b*) the concentration profile extracted from (*a*) is shown. (*c*) shows the front position extracted from (*b*) by finding the maximum of the concentration gradient, shown in (*d*). Finally, (*e*, *f*) show the pressure inside the prism.

3.2. *Experimental results obtained with set-up II*

3.2.1. *Effect of osmosis*

Figure 5 shows the data collected using set-up II. In figure 5(*a*), a time series of pictures is depicted showing the refracted laser-light projected onto a screen, the time gap between each image being 1 day. Comparing the upper and lower parts of each picture, one generally observes a deflection to the right at the bottom, corresponding to a high sugar concentration at the bottom of the prism. In the intermediate region one sees a dip in the refracted light, corresponding to a strong concentration gradient. The dip gradually flattens while it advances upwards, representing a sugar front which advances while it broadens. This process can be seen directly in figure 5(*b*),
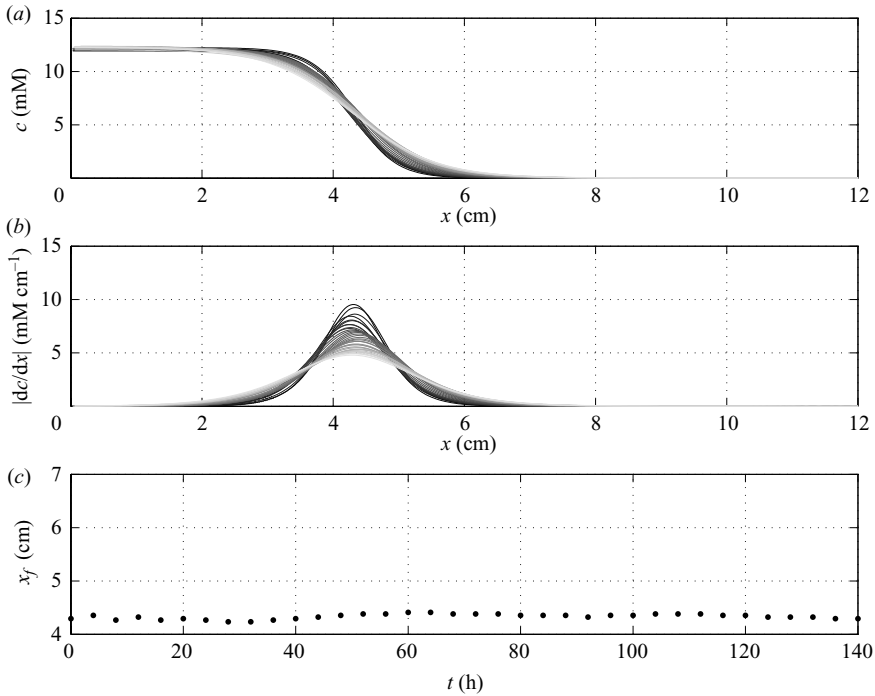
FIGURE 6. Results from a control experiment with set-up II, where concentration varies only due to diffusion. (*a*) Time evolution of the concentration profile, (*b*) time evolution of the profile of concentration gradient and (*c*) time evolution of the sugar front location.

which shows the time evolution of the sugar concentration obtained from the images. Starting from a steep concentration profile, we see that the front moves upwards while it flattens. In figure 5(*d*) the time evolution of the concentration gradient is depicted, clearly showing a peak which broadens while it moves forward. Finally, in figure 5(*e, f*), the position of the sugar front and the pressure inside the prism is plotted as a function of time. The error bars on x_f are ± 1 mm, as discussed below.

3.2.2. *Effect of diffusion*

To study the effect of diffusion on the dynamics of the sugar front separately, an experiment was made with set-up II, in which the water reservoir was not filled. The experiment was then conducted in the usual way, and the motion of the front was recorded. The results of this are shown in figure 6. Starting from a steep concentration gradient, we observe that the front flattens but otherwise does not move much.

Comparing figures 5 and 6 we observe, that while the front moves 2 cm due to osmosis in 6 days, it does not seem to move at all in 6 days due to diffusion. Thus, while diffusion has a flattening effect, it plays little role in the forward motion of the front.

Since the front did not move due to diffusion, the fluctuations in the front position seen in figure 6(*c*) gives a measure of the uncertainty of a single measurement of the front position. Taking the standard deviation of the fluctuations gives an uncertainty of ± 1 mm, shown as error bars in figure 5(*c*).

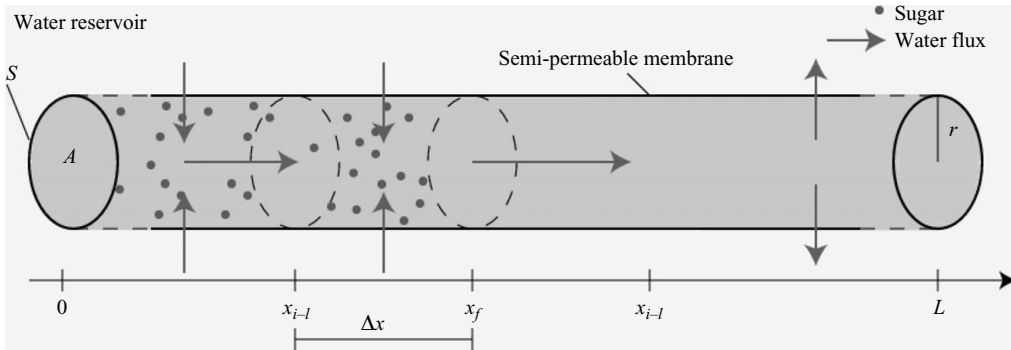More details on this second experiment can be found in Jensen (2007).

FIGURE 7. Sketch of the tube.

4. Theoretical analysis

4.1. *Front propagation via flow equations*

The equations of motion for osmotically driven flows have been derived and analysed thoroughly several times in the literature (Weir 1981) and have been studied carefully numerically (Henton 2002; Thompson & Holbrook 2003*a, b*). For the sake of completeness, we shall include a short derivation of these.

We consider a tube of length L and radius r, as shown in figure 7. The tube has a constant cross-section of area $A = \pi r^2$ and circumference $S = 2\pi r$ and its walls are made of a semi-permeable membrane with permeability κ. Inside the tube is a solution of sugar in water with concentration $c(x) = c(x, t)$. Throughout this paper, we study the transient dynamics generated by an asymmetrical initial concentration distribution, where the sugar is initially localized to one end of the tube with a concentration level c_0. The tube is surrounded by a water reservoir, modelling the water surrounding the membrane tube in set-up I.

We shall assume that $L \gg r$ and that the radial component of the flow velocity inside the tube is much smaller than the axial component, as is indeed the case in the experiments. With these assumptions, we will model the flow in the spirit of lubrication theory and consider only a single average axial velocity component $u(x, t)$. Also, we will assume that the concentration c is independent of the radial position ρ an assumption that can be verified experimentally in set-up II.

Let us now consider the equation for volume conservation by looking at a small section of the tube between x_{i-1} and x_i. The volume flux into the section due to advection is

$$A(u_{i-1} - u_i), \tag{4.1}$$

where the axial flow velocities are taken to be u_{i-1} and u_i at x_{i-1} and x_i, respectively. The volume flux inwards across the membrane due to osmosis (Schultz 1980) is

$$S \Delta x \kappa (RTc(x, t) - p(x, t)), \tag{4.2}$$

where p is the local difference of pressure across the membrane and c is the local concentration. For clarity we use the van't Hoff value $\Pi = RTc$ for the osmotic pressure, which is valid only for dilute (ideal) solutions. In appendix A.3, we show that the linear relation between Π and c is verified experimentally as $\Pi = (0.1 \pm 0.01$ bar mM^{-1})c. Assuming conservation of volume, we get

$$A(u_{i-1} - u_i) + S \Delta x \kappa (RTc - p) = 0. \tag{4.3}$$

Letting $\Delta x \to 0$ and using that the cross-section to perimeter ratio reduces to $r/2$, this becomes

$$\frac{r}{2}\frac{\partial u}{\partial x} = \kappa(RTc - p). \tag{4.4}$$

For these very slow and slowly varying flows, the time dependence of the Navier–Stokes equation can be neglected and the velocity field is determined by the instantaneous pressure gradient through the Poiseuille or Darcy relation (for a circular tube)

$$u = -\frac{r^2}{8\eta}\frac{\partial p}{\partial x}, \tag{4.5}$$

where η is the dynamic viscosity of the solution, typically $\sim 1.5 \times 10^{-3}$ Pa s in our experiments.

Differentiating (4.4) with respect to x and inserting the result from (4.5) we get for the conservation of water that

$$RT\frac{\partial c}{\partial x} = \frac{r}{2\kappa}\frac{\partial^2 u}{\partial x^2} - \frac{8\eta}{r^2}u. \tag{4.6}$$

The final equation expresses the conservation of sugar advected with velocity u and diffusing with molecular diffusivity D

$$\frac{\partial c}{\partial t} + \frac{\partial uc}{\partial x} = D\frac{\partial^2 c}{\partial x^2}. \tag{4.7}$$

The set of equations (4.6) and (4.7) is equivalent to those of Thompson & Holbrook (2003b) except for the fact that we have removed the pressure by substitution, and that we do not consider elastic deformations of the tube.

4.1.1. *Non-dimensionalization of the flow equations*

To non-dimensionalize (4.6) and (4.7), we introduce the following scaling

$$c = c_0C, \qquad u = u_0U, \qquad x = LX, \qquad t = t_0\tau,$$

L has been chosen such that the spatial domain is now of the unit interval $X \in [0, 1]$, $u_0 = L/t_0$ and c_0 is the initial concentration level in one end of the tube. Choosing further

$$t_0 = \frac{r}{2\kappa RTc_0}, \quad M = \frac{16\eta L^2\kappa}{r^3} \quad \text{and} \quad \bar{D} = \frac{D}{u_0L} = \frac{Dr}{2RTc_0L^2\kappa}, \tag{4.8}$$

and inserting in (4.6) and (4.7), we get the non-dimensional flow equations

$$\frac{\partial^2 U}{\partial X^2} - MU = \frac{\partial C}{\partial X}, \tag{4.9}$$

$$\frac{\partial C}{\partial \tau} + \frac{\partial UC}{\partial X} = \bar{D}\frac{\partial^2 C}{\partial X^2}. \tag{4.10}$$

The parameter M corresponds to the ratio of axial to membrane flow resistance, which we shall refer to as the *Münch number*. This is identical to the parameter $\hat{F}$ in Thompson & Holbrook (2003b). The second parameter $\bar{D}$ is the Peclet number. Thus, the longer the tube the less important the diffusion becomes and the more important the pressure gradient due to viscous effects becomes.

Values of the parameters M and $\bar{D}$ in different situations can be seen in table 3. The typical magnitude of the parameters M and $\bar{D}$ in plants are found from the

	M	$\bar{D}$
Set-up I	2×10^{-8}	6×10^{-5}
Set-up II	10^{-9}	2×10^{-2}
Single sieve element ($L = 1$ mm)	5×10^{-4}	5×10^{-4}
Leaf ($L = 1$ cm)	5×10^{-2}	5×10^{-5}
Branch ($L = 1$ m)	5×10^{2}	5×10^{-7}
Small tree ($L = 10$ m)	5×10^{4}	5×10^{-8}

TABLE 3. Values of the parameters M and $\bar{D}$ in various situations.

following values (also given in table 3):

$$r = 10\,\mu\text{m}, \quad \eta = 1.5 \times 10^{-3}\,\text{Pa s}, \quad u_0 = 2\,\text{m h}^{-1}, \quad \kappa = 2 \times 10^{-11}\,\text{m (Pa s)}^{-1}.$$

We observe, that M and $\bar{D}$ are small in both experiments, and that for short distance transport in plants this is also the case. However, over length scales comparable to a branch ($L = 1$ m) or a small tree ($L = 10$ m) M is large, so in this case the pressure gradient is not negligible.

When deriving the equations for osmotically driven flows, we have assumed that the concentration inside the tube was a function of x and t only. However, the real concentration inside the tube will also depend on the radial position ρ in the form of a concentration boundary layer near the membrane, in the literature called an *unstirred layer* (Pedley 1983). Close to the membrane, the concentration c_m is lowered compared to the bulk value c_b because sugar is advected away from the membrane by the influx of water. This, in turn, results in a lower influx of water, ultimately causing the axial flow inside the tube to be slower than expected. In our experiments we see no signs of such boundary layers and apparently their width and their effect on the bulk flow are very small.

5. Solutions of the flow equations

We will now analyse (4.9) and (4.10). We will show that they can be solved quite generally for $M = \bar{D} = 0$ by the method of characteristics. For an arbitrary initial condition, this method will generally yield an implicit solution.

For arbitrary values of M and $\bar{D}$, we cannot solve the equations of motion analytically and thus have to incorporate numerical methods. This topic has been the focus of much work both in the steady-state case (Thompson & Holbrook 2003a) and in the transient case (Henton 2002). However, no formulation fully exploiting the partially linear character of the equations capable of handling all different boundary conditions has so far been presented. Therefore, we show that using Green's functions, the equations of motion can be transformed into a single integro-differential equation, which can be solved using standard numerical methods with very high precision. This technical numerical part is detailed in appendix B.

5.1. *Results for small Münch number*

In the limit $M = \bar{D} = 0$ the equations become

$$\frac{\partial^2 U}{\partial X^2} = \frac{\partial C}{\partial X}, \tag{5.1}$$

$$\frac{\partial C}{\partial \tau} + \frac{\partial U C}{\partial X} = 0. \tag{5.2}$$

By integrating (5.1) with respect to X, we get

$$\frac{\partial U}{\partial X} = C + F(\tau).$$
(5.3)

If we choose $U(0) = U(1) = 0$, $F(\tau)$ becomes

$$F(\tau) = -\int_0^1 C \, \mathrm{d}X \equiv -\bar{C}(\tau).$$
(5.4)

Using (5.3) in (5.2) gives

$$\frac{\partial}{\partial X}\left[\frac{\partial U}{\partial \tau} + U\left(\frac{\partial U}{\partial X} + \bar{C}\right)\right] = -\frac{\mathrm{d}\bar{C}}{\mathrm{d}\tau} = 0,$$
(5.5)

where the last equality follows from integrating X from 0 to 1, observing that all terms in the square bracket vanish at the end points due to the boundary condition $u(X = 0, \tau) = u(X = 1, \tau) = 0$. Thus $\bar{C}$ is a constant in time since the tube is closed. Integrating with respect to X and using the boundary conditions on U, this becomes

$$\frac{\partial U}{\partial \tau} + U\frac{\partial U}{\partial X} = -\bar{C}U.$$
(5.6)

Equation (5.6) is a damped Burgers equation (Gurbatov, Malakhov & Saichev 1991), which can be solved using Riemann's method of characteristics. The characteristic equations are

$$\frac{\mathrm{d}U}{\mathrm{d}\tau} = -\bar{C}U$$
(5.7)

$$\frac{\mathrm{d}X}{\mathrm{d}\tau} = U.$$
(5.8)

Equation (5.7) has the solution

$$U = U_0(\xi)\exp(-\bar{C}\tau),$$
(5.9)

where the parametrization $\xi(X, \tau)$ of the initial velocity has to be found from

$$X = \xi + \frac{1}{\bar{C}}U_0(\xi)(1 - \exp(-\bar{C}\tau)),$$
(5.10)

where $\xi = X$ at $\tau = 0$.

5.1.1. *Exact solutions for simple initial conditions*

An experimental condition close to that of our experiments is to use a Heaviside step function as initial condition on C, making C initially constant in some interval $[0, \lambda]$

$$C(X, \tau = 0) = C_I H(\lambda - X) = \begin{cases} C_I & \text{for} \quad 0 \leqslant X \leqslant \lambda. \\ 0 & \text{for} \quad \lambda < X \leqslant 1. \end{cases}$$
(5.11)

Equation (5.3) now enables us to find the initial condition on the velocity

$$U(X, \tau = 0) = \int_0^X (C(X', 0) - \bar{C}) \, \mathrm{d}X' = \int_0^X (C(X', 0) - \lambda C_I) \, \mathrm{d}X'$$
(5.12)

$$= \begin{cases} (C_I - \bar{C})X & \text{for} \quad 0 \leqslant X \leqslant \lambda. \\ \bar{C}(1 - X) & \text{for} \quad \lambda < X \leqslant 1. \end{cases}$$
(5.13)

From (5.13), we have

$$U_0(\xi) = \begin{cases} (C_I - \bar{C})\xi & \text{for} \quad 0 \leqslant \xi \leqslant \lambda. \\ \bar{C}(1 - \xi) & \text{for} \quad \lambda < \xi \leqslant 1. \end{cases} \tag{5.14}$$

Then, solving for $\xi(X, \tau)$ in (5.10) gives

$$\xi(X, \tau) = \begin{cases} \dfrac{X}{1 + (1/\lambda)(1 - \lambda)(1 - \exp(-\bar{C}\tau))} & \text{for} \quad X \in I_1, \\ \dfrac{X - 1 + \exp(-\bar{C}\tau)}{\exp(-\bar{C}\tau)} & \text{for} \quad X \in I_2, \end{cases} \tag{5.15}$$

where the intervals I_1 and I_2 are defined by

$$I_1 = [0, 1 - (1 - \lambda)\exp(-\bar{C}\tau)], \tag{5.16}$$
$$I_2 = [1 - (1 - \lambda)\exp(-\bar{C}\tau), 1]. \tag{5.17}$$

Finally, $U(X, \tau)$ is calculated from (5.9)

$$U(X, \tau) = \begin{cases} \dfrac{(C_I - \bar{C})\exp(-\bar{C}\tau)X}{(1/\lambda)(1 - \lambda)(1 - \exp(-\bar{C}\tau))} & \text{for} \quad X \in I_1, \\ \bar{C}(1 - X) & \text{for} \quad X \in I_2, \end{cases} \tag{5.18}$$

which is equivalent to the result obtained by Weir (1981). The solution is plotted in figure 8(a, b). We can now calculate the instantaneous sugar front position X_f and velocity U_f using the right boundary of I_1 from (5.16)

$$X_f(\tau) = 1 - (1 - \lambda)\exp(-\bar{C}\tau), \tag{5.19}$$
$$U_f(\tau) = \frac{dX_f}{d\tau} = \bar{C}(1 - \lambda)\exp(-\bar{C}\tau). \tag{5.20}$$

Similarly, $C(X, \tau)$ is given by

$$C(X, \tau) = \frac{\bar{C}}{1 - (1 - \lambda)\exp(-\bar{C}\tau)} H(X_f - X). \tag{5.21}$$

Going back to dimensional variables, (5.19) and (5.20) become

$$x_f(t) = L - (L - l)\exp\left(-\frac{t}{t_0}\right) \quad \text{and} \tag{5.22}$$
$$u_f(t) = \frac{L}{t_0}\exp\left(-\frac{t}{t_0}\right), \tag{5.23}$$

where L is the length of the membrane tube, l is the initial front position and the decay time t_0 is in accordance with the simple argument given in §1.

As noted earlier we can use the method of characteristics on arbitrary initial conditions, including the more realistic case, where the initial jump in concentration is replaced by a continuous variation, say, a linear decrease from C_I to 0 taking place between λ_1 and λ_2, i.e.

$$C(X, \tau = 0) = \begin{cases} C_I & \text{for} \quad 0 \leqslant X \leqslant \lambda_1. \\ C_I \dfrac{\lambda_2 - X}{\lambda_2 - \lambda_1} & \text{for} \quad \lambda_1 \leqslant X \leqslant \lambda_2. \\ 0 & \text{for} \quad \lambda_2 < X \leqslant 1. \end{cases} \tag{5.24}$$
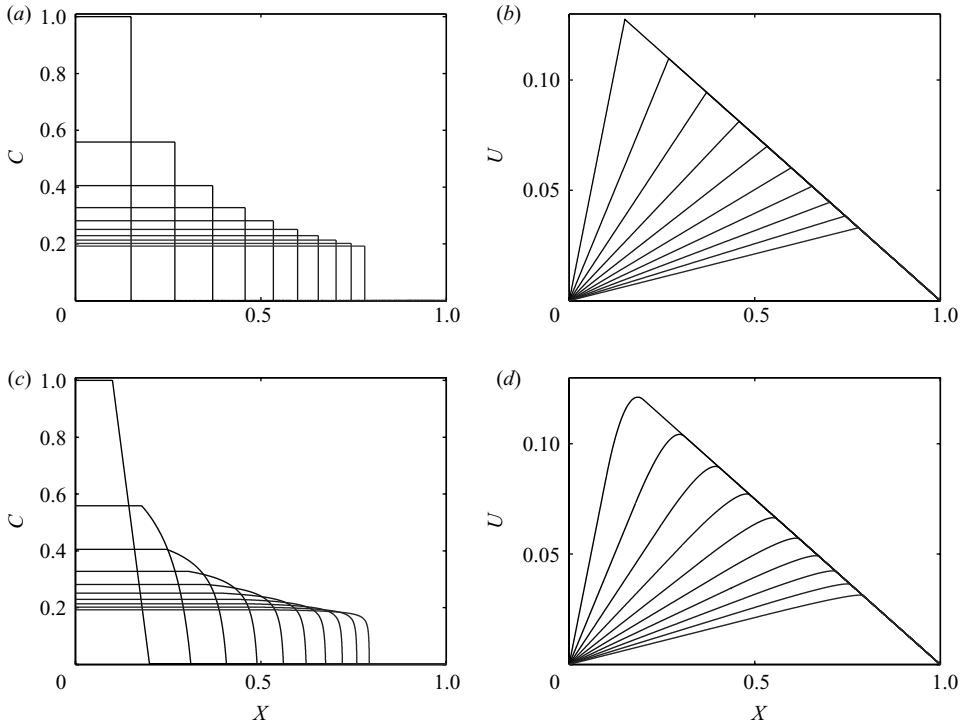
FIGURE 8. (a, b) Plot of the analytical solution for a piecewise constant initial concentration. $\lambda = 0.1$, $C_I = 1$ and $\bar{C} = 0.1$. (c, d) Plot of the analytical solution for a piecewise linear initial concentration. $\lambda_1 = 0.05$, $\lambda_2 = 0.15$, $C_I = 1$ and $\bar{C} = 0.1$. Time increases from black to gray in steps of one unit of time.

Using (5.3) yields the initial velocity

$$
U(X, \tau = 0) = \begin{cases} (C_I - \bar{C})X & \text{for} \quad 0 \leqslant X \leqslant \lambda_1, \\ A_1 X^2 + B_1 X + C_1 & \text{for} \quad \lambda_1 \leqslant X \leqslant \lambda_2, \\ \bar{C}(1 - X) & \text{for} \quad \lambda_2 < X \leqslant 1, \end{cases} \tag{5.25}
$$

where $\bar{C} = C_I(\lambda_1 + \lambda_2)/2$, and the constants are given by

$$
A_1 = -\frac{C_I}{2(\lambda_2 - \lambda_1)}, \quad B_1 = \frac{C_I \lambda_2}{\lambda_2 - \lambda_1} - \bar{C}, \quad C_1 = C_I \lambda_1 + \frac{C_I}{\lambda_2 - \lambda_1}\left(\lambda_1 \lambda_2 + \lambda_1^2/2\right). \tag{5.26}
$$

Finding $\xi(X, \tau)$ from (5.10) now gives

$$
\xi(X, \tau) = \begin{cases} \dfrac{X}{1 + (1/\lambda)(1 - \lambda)(1 - \exp(-\bar{C}\tau))} & \text{for} \quad X \in I_1, \\ A_2 \xi_2^2 + B_2 \xi_2^2 + C_2 & \text{for} \quad X \in I_2, \\ \dfrac{X - 1 + \exp(-\bar{C}\tau)}{\exp(-\bar{C}\tau)} & \text{for} \quad X \in I_3, \end{cases} \tag{5.27}
$$

where

$$
A_2 = \frac{A_1}{\bar{C}}(1 - \exp(-\bar{C}\tau)), \quad B_2 = 1 + \frac{B_1}{\bar{C}}(1 - \exp(-\bar{C}\tau)), \quad C_2 = \frac{C_1}{\bar{C}}(1 - \exp(-\bar{C}\tau)). \tag{5.28}
$$

Here

$$\xi_2 = \frac{-B_2 + \sqrt{B_2^2 - 4A_2(C_2 - X)}}{2A_2}, \tag{5.29}$$

where the plus solution has been chosen to ensure that $\xi \to X$ as $\tau \to 0$. Finally,

$$I_1 = \left[0, \lambda_1 + \frac{\lambda_1}{\bar{C}}(C_I - \bar{C})(1 - \exp(-\bar{C}\tau))\right], \tag{5.30}$$

$$I_2 = \left[\lambda_1 + \frac{\lambda_1}{\bar{C}}(C_I - \bar{C})(1 - \exp(-\bar{C}\tau)), 1 + (\lambda_2 - 1)\exp(-\bar{C}\tau)\right], \tag{5.31}$$

$$I_3 = \left[1 + (\lambda_2 - 1)\exp(-\bar{C}\tau), 1\right]. \tag{5.32}$$

Plugging into (5.9) gives $U(X, \tau)$ as

$$U(X, \tau) = \begin{cases} \dfrac{(C_I - \bar{C})\exp(-\bar{C})X}{1 + (1/\lambda)(1 - \lambda)(1 - \exp(-\bar{C}\tau))} & \text{for} \quad X \in I_1, \\ \left(A_1\xi_2^2 + B_1\xi_2^2 + C_1\right)\exp(-\bar{C}\tau) & \text{for} \quad X \in I_2, \\ \bar{C}(1 - X) & \text{for} \quad X \in I_3, \end{cases} \tag{5.33}$$

as shown in figure 8 along with C found from (5.3), i.e.

$$C = \frac{\partial U}{\partial X} + \bar{C}. \tag{5.34}$$

Note that the interval I_2 does not shrink to 0 in time ($I_2 \to [\lambda_1 C_1/\bar{C}, 1]$ for $\tau \to \infty$), but the curvature around the right-hand end point grows without bound so that the limiting shape of the concentration profile again becomes a discontinuous Heaviside function.

5.2. *Results for large Münch number*

In the limit of large $M \gg 1$ we cannot neglect the pressure gradient along the channel and this term dominates the advective term in (4.9), i.e. the second derivative in U. Thus

$$\frac{\partial C}{\partial X} = -MU \tag{5.35}$$

$$\frac{\partial C}{\partial \tau} + \frac{\partial CU}{\partial X} = \bar{D}\frac{\partial^2 C}{\partial X^2} \tag{5.36}$$

giving the nonlinear diffusion equation

$$\frac{\partial C}{\partial \tau} = M^{-1}\frac{\partial}{\partial X}\left[C\frac{\partial C}{\partial X}\right] + \bar{D}\frac{\partial^2 C}{\partial X^2}. \tag{5.37}$$

If we neglect molecular diffusion the resulting universal nonlinear diffusion equation can be written as

$$\frac{\partial C}{\partial \tau} = M^{-1}\frac{\partial}{\partial X}\left[C\frac{\partial C}{\partial X}\right]. \tag{5.38}$$

This can be done as long as $M^{-1}C \gg \bar{D} \approx 10^{-5}$. If M becomes even larger normal diffusion will take over. Equation (5.38) belongs to a class of equations which have been studied, e.g. in the context of intense thermal waves by Zeldovich *et al.* and flow through porous media by Barenblatt (1996) in the 1950s. The Münch number M can be removed by rescaling the time according to $\tau = Mt$, so when M is large we get

very slow motion with a time scale growing linearly with M. Equation (5.38) admits scaling solutions of the form

$$C(X, \tau) = \left(\frac{\tau}{M}\right)^{\alpha} \Phi(\xi) \quad \text{with} \quad \xi = X \left(\frac{\tau}{M}\right)^{\beta} \tag{5.39}$$

as long as $\alpha + 2\beta + 1 = 0$. The total amount of sugar is, however, conserved. In our rescaled units

$$\int_0^1 C(X, \tau) \, \mathrm{d}X = \lambda, \tag{5.40}$$

where, as before, λ is the fraction of the tube initially containing the sugar. We can only hope to find a scaling solution in the intermediate time regime, where the precise initial condition has been forgotten, but the far end ($X = 1$) is not yet felt. Thus we can replace integral (5.40) with

$$\int_0^{\infty} C(X, \tau) \, \mathrm{d}X = \lambda \tag{5.41}$$

which implies that $\alpha = \beta = -1/3$ and

$$C(X, \tau) = \left(\frac{\tau}{M}\right)^{-1/3} \Phi(\xi) \quad \text{with} \quad \xi = X \left(\frac{\tau}{M}\right)^{-1/3}. \tag{5.42}$$

Inserting this form into (5.38), we obtain the differential equation for Φ

$$\frac{1}{2} \frac{\mathrm{d}^2 \Phi^2}{\mathrm{d}\xi^2} + \frac{1}{3} \frac{\mathrm{d}(\xi \Phi)}{\mathrm{d}\xi} = 0 \tag{5.43}$$

which can be integrated once to

$$\Phi \frac{\mathrm{d}\Phi}{\mathrm{d}\xi} + \frac{1}{3} \xi \Phi = \text{constant}. \tag{5.44}$$

Due to the boundary condition $\partial C / \partial X = 0$ in the origin, the constant has to vanish and we find the solution

$$\Phi(\xi) = \frac{1}{6}(b^2 - \xi^2) \tag{5.45}$$

which is valid only for ξ smaller than the constant b. For $\xi > b$, Φ is identically 0. The fact that the solution – in contrast to the linear diffusion equation – has *compact support*, is an interesting characteristic of a large class of nonlinear diffusion equations (Barenblatt 1996). The value of b is determined by conservation integral (5.41) giving $\int_0^{\infty} \Phi \, \mathrm{d}\xi = 1$, and thus $b = (9\lambda)^{1/3}$.

The final solution thus has the form

$$C(X, \tau) = \begin{cases} \dfrac{M}{6\tau}((X_f(\tau))^2 - X^2) & \text{for} \quad X < X_f(\tau) = \left(9\lambda \dfrac{\tau}{M}\right)^{1/3} \\ 0 & \text{for} \quad X > X_f(\tau) \end{cases} \tag{5.46}$$

which shows that the sugar front moves as $X_f(\tau) \sim \tau^{1/3}$ and the concentration at the origin decays as $C(0, \tau) \sim \tau^{-1/3}$. To check the validity of this solution, also when the initial condition has support in a finite region near the origin, we plot $(\tau/M)^{1/3} C(X, \tau)$ against $\xi = X(\tau/M)^{-1/3}$ in figure 9(c). The corresponding solution for U is found from
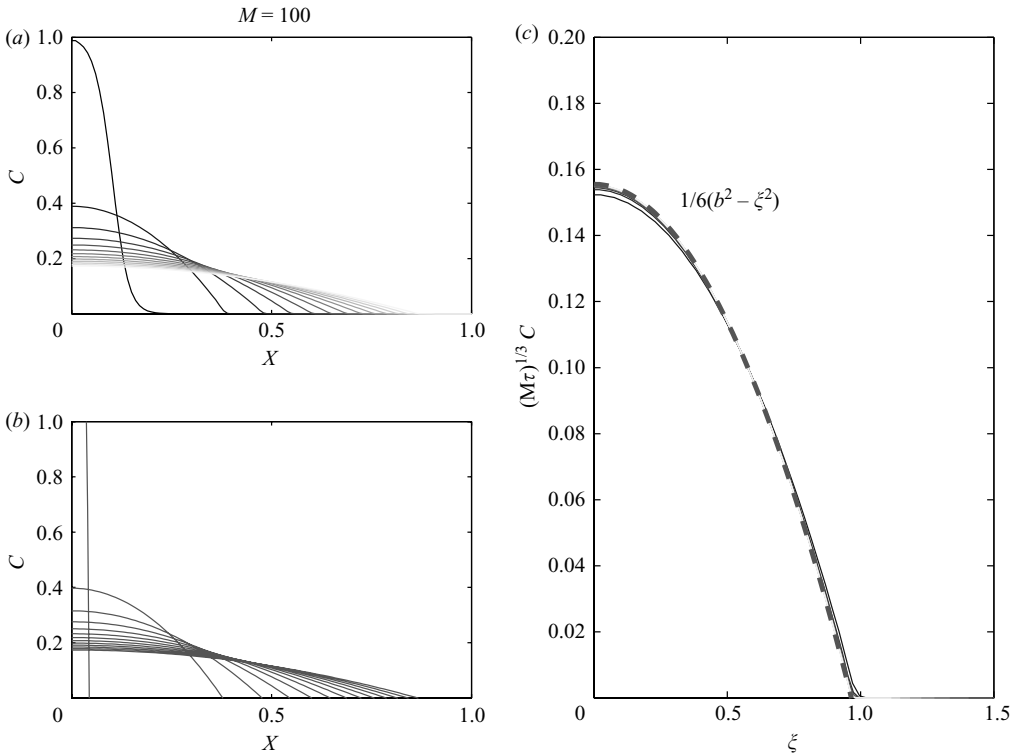
FIGURE 9. (*a*) Numerical simulation of (5.38) compared with (*b*) scaling solution (5.46) and (*c*) (5.45), which is shown as a dashed line. The initial condition has the form $C(X, 0) = 1 - [1 + \exp(-(X - \lambda)/\epsilon)]^{-1}$, where $\lambda = 0.1$ and $\epsilon = 2 \times 10^{-2}$ and the curves are equidistant in time. When λ controlling the size of the region of non-zero initial sugar concentration becomes larger, a more accurate scaling solution is found by letting $\tau \to \tau + \tau_0$ and treating τ_0 as an unknown parameter. In (*c*), we have omitted the first curve (the initial condition).

(5.35) as

$$U(X, \tau) = \begin{cases} \dfrac{X}{3\tau} & \text{for} \quad X < X_f(\tau) \\ 0 & \text{for} \quad X > X_f(\tau) \end{cases} \tag{5.47}$$

and $\partial^2 U/\partial X^2 = 0$ justifying the neglect of $\partial^2 U/\partial X^2$ in going from (4.9) to (5.35) for large M. It is seen that the velocity of the sugar front $X'_f(\tau) = (\lambda/(3M))^{1/3}\tau^{-2/3}$ is identical to $U(X_f(\tau), \tau)$ from (5.47).

6. Comparison between theory and experiment

In §§ 2.2 and 3.2, we have presented experiments demonstrating the movement of a sugar solution inside a membrane tube surrounded by a reservoir of water. We now wish to consider whether the theory is in agreement with the experimental results.

6.1. *Set-up I*

The plot in figure 10 shows the relative front position, $(L - x_f)/(L - l)$, plotted against time for five different experiments conducted with set-up I. The numbers 1–5 indicate the sugar concentrations used (cf. table 2). One clearly sees, that the relative front position approaches zero faster for high concentrations than for low. Typical
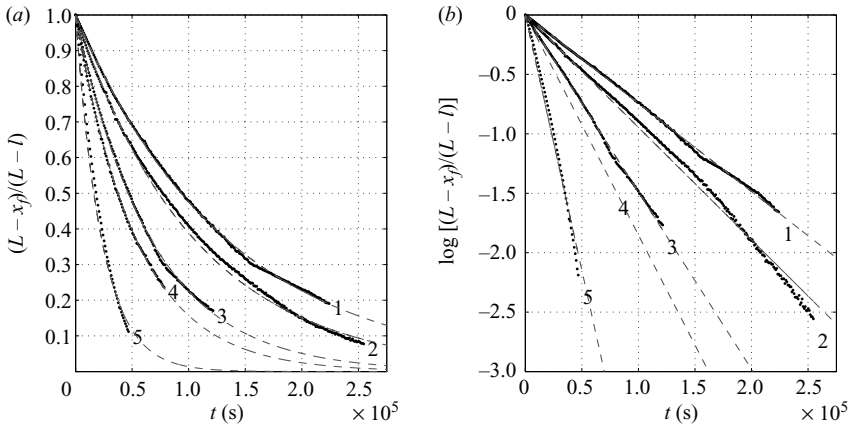
FIGURE 10. (a) Experimental (black dots) and fits to (5.22) for the relative front position versus time, shown as dashed lines. (b) Semi-logarithmic version of (a).
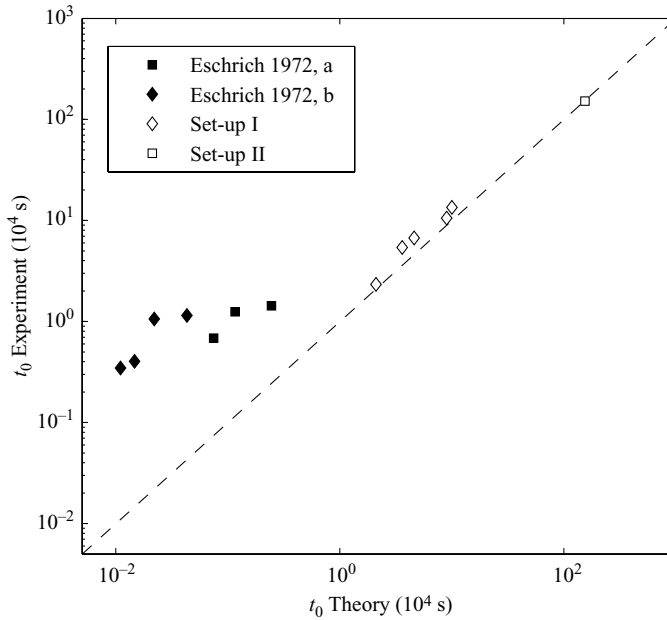

FIGURE 11. Our experimentally obtained values of t_0 plotted together with the results found by Eschrich et al. (1972). Data points marked with an 'a' represent results from closed tube experiments and points marked with a 'b' represent results from semi-closed experiments taken from figures 8 and 9 of the original paper.

values of M and $\bar{D}$ are $M \sim 10^{-8}$ and $\bar{D} \sim 10^{-5}$, so it is reasonable to assume that we are in the domain where the analytical solution for $M = \bar{D} = 0$ is valid. To test the result from (5.19) against the experimental data, the plot in figure 10 shows the logarithm of the relative front position plotted against time. For long stretches of time the curves are seen to approximately follow straight lines in good qualitative agreement with theory. The dashed lines are fits to (5.19), and we interpret the slopes as $-\frac{1}{t_0}$, the different values plotted in figure 11 against the theoretical values. The theoretically and experimentally obtained values of t_0 are in good quantitative
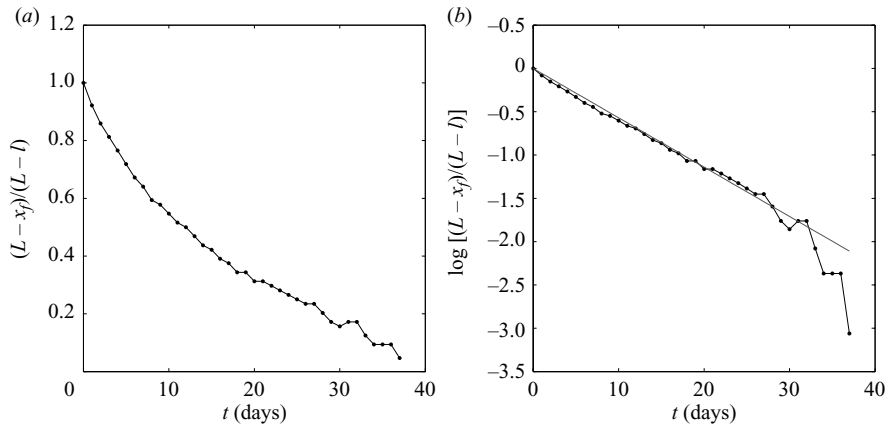
FIGURE 12. (*a*) Experimental data obtained using set-up II showing the relative front position (black dots) as a function of time. (*b*) Lin–log plot of the experimental data shown on the left. The solid line is a fit to (5.22) with $t_0 = 1.6 \times 10^6$ s.

agreement, within 10 %–30 %. Generally, theory predicts somewhat smaller values of t_0 than observed, implying that the observed motion of the sugar front is a little slower than expected from the pressure-flow hypothesis. Nevertheless, as can be seen in figure 11 these results are a considerable improvement to the previous results obtained by Eschrich *et al.* as we find much better agreement between experiment and theory.

6.2. *Set-up II*

The plot in figure 12 shows the relative front position, $(L - x_f)/(L - l)$, plotted against time for the experiment conducted with set-up I. On the semi-logarithmic plot, the curves are seen to follow straight lines in good qualitative agreement with the simple theory for $M = \bar{D} = 0$. As can be seen in figure 11, we also found very good quantitative agreement between the experiment and theory for set-up II.

To test how well the motion of the sugar front observed in the experiments with set-up II was reproduced by our model, we solved the equations of motion numerically starting with the initial conditions from figure 5. For $M = \bar{D} = 0$, the results are shown in figure 13(*b*). While the front positions are reproduced relatively well, the shape of the front is not, so diffusion must play a role. This can be seen in figure 13(*c*) which shows the result of simulation with $M = 10^{-9}$, $D = 6.9 \times 10^{-11}$ m^2 s^{-1}. Clearly, the model which includes diffusion reproduces the experimental data significantly better.

To study the shape of the front in greater detail, consider the plots in figure 13(*d–f*). Here the gradient of the concentration curves on the left in figure 13 is shown. In figure 13(*d*) we clearly see a peak moving from left to right while it gradually broadens and flattens. In figure 13(*e*) also we see the peak advancing, but the flattening and broadening is much less pronounced. In figure 13(*f*) we see that the model which includes diffusion reproduces the gradual broadening and flattening of the front very well.

7. Conclusion

In this paper we have studied osmotically driven transient pipe flows. The flows are generated by concentration differences of sugar in closed tubes, fully or partly
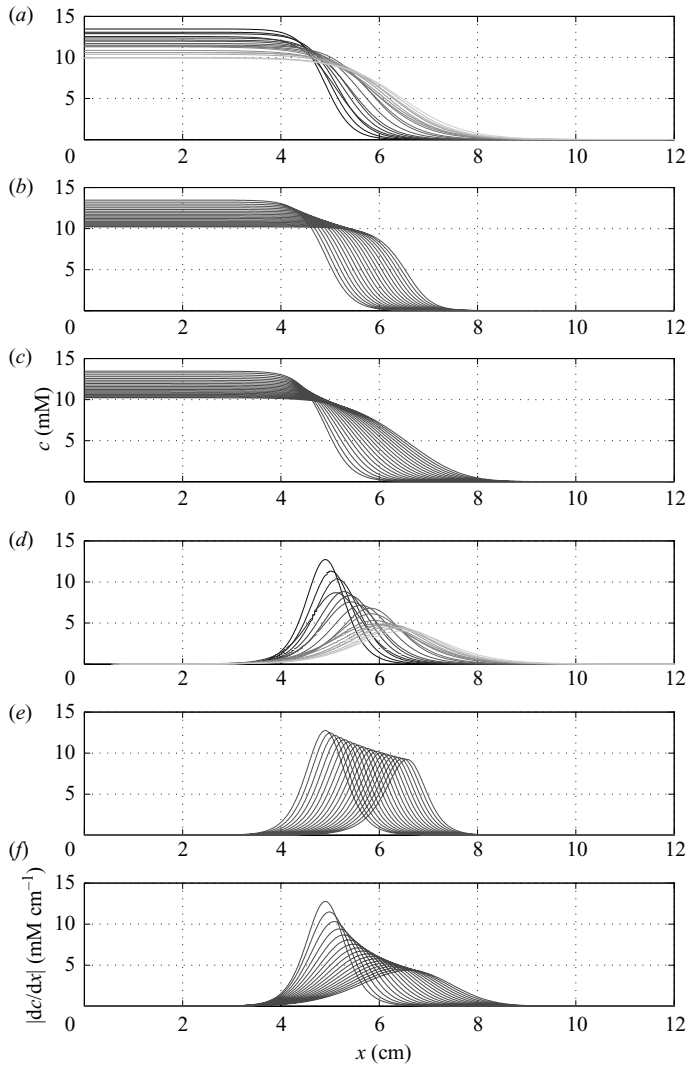
FIGURE 13. Results from set-up II showing the experimental data (a, d) and the numerical model for $M = D = 0$ (b, e) and for $M = 10^{-9}$, $D = 6.9 \times 10^{-11}$ m^2 s^{-1} (c, f).

enclosed by semi-permeable membranes surrounded by pure water. The flows are initiated by a large concentration in one end of the tube and we study the approach to equilibrium, where the sugar is distributed evenly within the tube. Experimentally, we have used two configurations: the first is an updated version of the set-up of Eschrich *et al.* where the flow takes place in a dialysis tube and the sugar is followed by introducing a dye. The advantage is the relatively rapid motion, due to the large surface area. The disadvantage is that the sugar concentration cannot be inferred accurately by this method and for this reason we have introduced our second set-up, where the sugar concentration can be followed directly by refraction measurements.

On the theoretical side, we first re-derive the governing flow equations and introduce the dimensionless Münch number M. We then show that analytical solutions can be obtained in the two important limits of very large and very small M. In the general case we show how numerical methods based on Green's functions are very effective.

Finally, we compare theory and experiment with very good agreement. In particular the results or the velocity of the front (as proposed by Eschrich *et al.*) can be verified rather accurately.

Concerning the application to sap flow, the quantitative study we performed leads to the following conclusions: for a large tree it seems improbable that sugar transport, e.g. from leaf to root by this sole passive mechanism would be sufficiently efficient. In this case active transport processes might play an important role. On the other hand, transport over short distances, e.g. locally in leaves or from a leaf to a nearby shoot might be more convincingly described by the pressure-flow hypothesis.

Appendix A. Materials: sugar and membrane

A.1. *Sugar*

The sugar used was a dextran (Sigma-Aldrich, St Louis, MO, USA, type D4624) with an average molecular weight of 17.5 kDa. The dye used was a red fruit dye (Flachsmann Scandinavia, Rød Frugtfarve, type 123000) consisting of an aqueous mixture of the food additives E-124 and E-131 with molecular weights of 539 Da and 1159 Da, respectively (PubChem-Database 2007). Even though the molecular weights are below the MWCO of the membrane, the red dye was not observed to leak through the membrane. This, however, was observed when using another type of dye, Methylene blue, which has a molecular weight of 320 Da.

A.2. *Membrane*

The membrane used in both set-ups was a semi-permeable dialysis membrane tube (Spectra/Por Biotech cellulose ester dialysis membrane) with a radius of 5 mm, a thickness of 60 μm and a MWCO (molecular weight cut off) of 3.5 kDa. The permeability L_p was determined by applying a pressure and measuring the flow rate across the membrane

$$L_p = (1.8 \pm 0.2) \times 10^{-12} \, \text{m} \, (\text{Pa} \, \text{s})^{-1}. \tag{A 1}$$

A.3. *Osmotic strength of dextran*

Figure 14(left) shows the relation between dextran concentration and osmotic pressure found from the experiments shown in figure 3. A linear fit gives

$$\Pi = (0.1 \pm 0.01 \, \text{bar} \, \text{mM}^{-1})c \tag{A 2}$$

where Π has unit bar, and c is measured in mM. This is in good agreement with values given by Jonsson (1986).

Appendix B. Numerical methods for non-zero M and $\bar{D}$

For non-zero values of M and $\bar{D}$, the equations of motion,

$$\frac{\partial^2 U}{\partial X^2} - MU = \frac{\partial C}{\partial X} \tag{B 1}$$
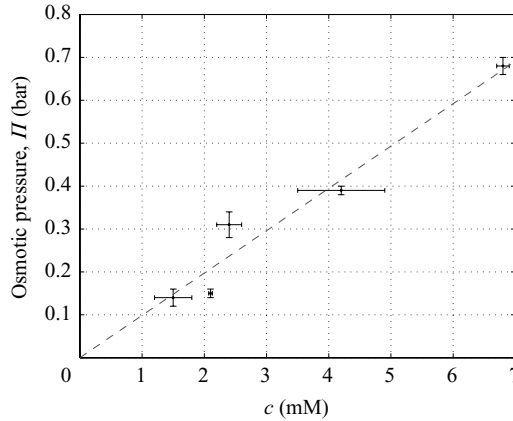
FIGURE 14. van't Hoff relation for 17.5 kDa dextran.

and

$$\frac{\partial C}{\partial \tau} + \frac{\partial C U}{\partial X} = \bar{D} \frac{\partial^2 C}{\partial X^2} \tag{B2}$$

cannot be solved analytically. However, they can be written as a single integro-differential equation, which is straightforward to solve on a computer. If we choose a set of linear boundary conditions, $B_X[U] = a_i$, for (B1), the solution can be written as

$$U = \int_0^1 G(X, \xi) \frac{\partial C}{\partial \xi} d\xi + U_2. \tag{B3}$$

Here, $G(X, \xi)$ is the Green's function for the differential operator $\partial^2/\partial X^2 - M$ with boundary conditions $B_X[U] = 0$ and U_2 fulfils the homogeneous version of (B1) with $B_X[U] = a_i$. Plugging this into (B2) yields

$$\frac{\partial C}{\partial \tau} + \frac{\partial}{\partial X} \left(C \left(\int_0^1 G(X, \xi) \frac{\partial C}{\partial \xi} d\xi + U_2 \right) \right) = \bar{D} \frac{\partial^2 C}{\partial X^2}. \tag{B4}$$

For the closed tube, i.e. for the boundary conditions $U(0, \tau) = U(1, \tau) = 0$, $G(X, \xi)$ is given by

$$G(X, \xi) = \begin{cases} -\dfrac{\sinh(a(1 - X))}{a \sinh a} \sinh a\xi & \text{for} \quad \xi < X, \\ -\dfrac{\sinh aX}{a \sinh a} \sinh(a(1 - \xi)) & \text{for} \quad \xi > X, \end{cases} \tag{B5}$$

and $U_2 = 0$. To increase numerical accuracy, it is convenient to transform (B4) by defining

$$\frac{\partial f}{\partial X} = C - \bar{C} \tag{B6}$$

and choosing $f(0) = f(1) = 0$ such that $f(X) = \int_0^X (C - \bar{C}) d\xi$. Inserting in (B4), we get

$$\frac{\partial f}{\partial t} = \bar{D} \frac{\partial^2 f}{\partial X^2} - \left(f(X) - \int_0^1 \frac{\partial K(X, \xi)}{\partial \xi} f(\xi) d\xi \right) \left(\frac{\partial f}{\partial X} + \bar{C} \right), \tag{B7}$$
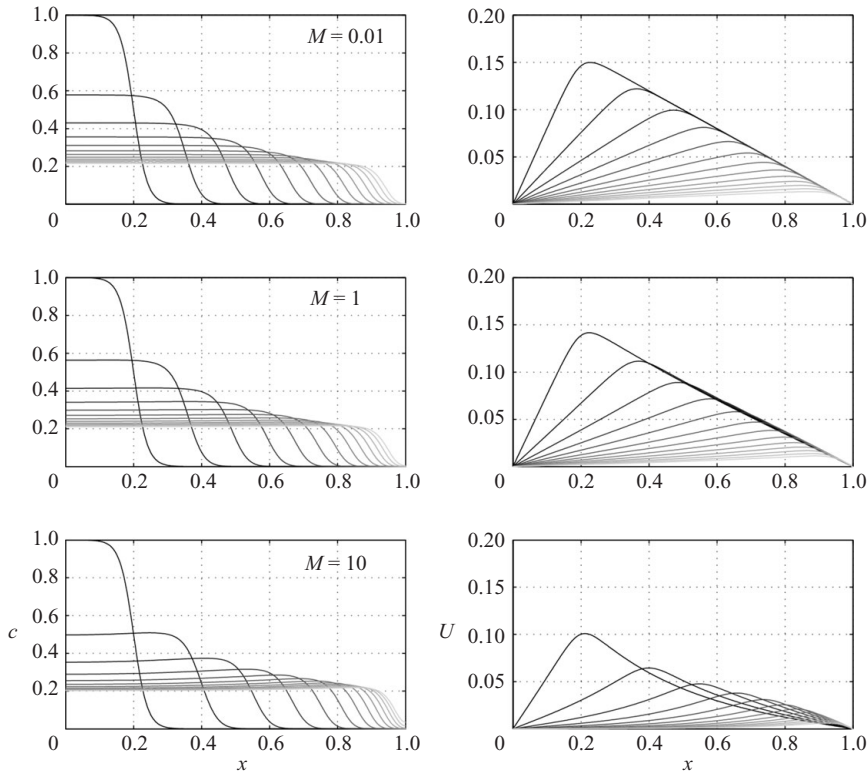
FIGURE 15. Results of numerical simulation of (B 4) using the boundary conditions $U(0, \tau) = U(1, \tau) = 0$ for different values of M. $\bar{D}$ is kept constant at 10^{-5}. The initial condition was $C(X, 0) = 1 - 1/(1 + \exp(-(X - \lambda)/\epsilon))$ where $\lambda = 0.2$ and $\epsilon = 2 \times 10^2$.

where

$$
\frac{\partial K(X, \xi)}{\partial \xi} = \begin{cases} -a\dfrac{\sinh(a(1 - X))}{\sinh a} \sinh a\xi & \text{for} \quad \xi < X, \\ -a\dfrac{\sinh aX}{\sinh a} \sinh(a(1 - \xi)) & \text{for} \quad \xi > X. \end{cases} \tag{B 8}
$$

To solve (B 7) we used MATLAB's built-in time solver ode23t which is based on an explicit Runge–Kutta formula along with standard second-order schemes for the first- and second-order derivatives. For the spatial integration, the trapezoidal rule was used (Press 2001). Results of a numerical simulation for different values of M are shown in figure 15.

REFERENCES

BARENBLATT, G. I. 1996 *Scaling, Self-Similarity, and Intermediate Asymptotics*. Cambridge University Press.

ESCHRICH, W., EVERT, R. F. & YOUNG, J. H. 1972 Solution flow in tubular semipermeable membranes. *Planta(Berl.)* **107**, 279–300.

FRISCH, H. L. 1976 Osmotically driven flow in narrow channels. *Trans. Soc. Rheol.* **20**, 23–27.

GURBATOV, S. N. MALAKHOV, A. N. & SAICHEV, A. I. 1991 *Nonlinear Random Waves and Turbulence in Nondispersive Media: Waves, Rays, Particles*. Manchester University Press.

K. H. Jensen, E. Rio, R. Hansen, C. Clanet and T. Bohr

HENTON, S. M. 2002 Revisiting the Münch pressure-flow hypothesis for long-distance transport of carbohydrates: modelling the dynamics of solute transport inside a semipermeable tube. *J. Exp. Bot.* **53**, 1411–1419.

JONSSON, G. 1986 Transport phenomena in ultrafiltration: membrane selectivity and boundary layer phenomena. *J. Pure Appl. Chem.* **58**, 1647–1656.

JENSEN, K. H. 2007 Osmotically driven flows and their relation to sugar transport in plants. MSc Thesis, The Niels Bohr Institute, University of Copenhagen.

KNOBLAUCH, M. & VAN BEL, A. J. E. 1998 Sieve tubes in action. *The Plant Cell* **10**, 35–50.

LANDAU, L. D. & LIFSHITZ, E. M. 1980 *Statistical Physics*. Pergamon Press.

MÜNCH, E. 1930 *Die Stoffbewegung in der Pflanze*. Verlag von Gustav Fisher.

NIKLAS, K. J. 1992 *Plant Biomechanics – An Engineering Approach to Plant Form and Function*. The University of Chicago Press.

NOBEL, P. S. 1999 *Physicochemical & Environmental Plant Physiology*. Academic Press.

PEDLEY, T. J. 1983 Calculation of unstirred layer thickness in membrane transport experiments: a survey. *Quart. Rev. Biophys.* **16**, 115–150.

PRESS, W. H. 2001 *Numerical Recipes in Fortran 77*, Vol. 1 Cambridge University Press.

PUBCHEM–DATABASE 2007 http://pubchem.ncbi.nlm.nih.gov/ *National Library of Medicine*

SCHULTZ, S. G. 1980 *Basic Principles of Membrane Transport*. Cambridge University Press.

TAIZ, L. & ZEIGER, E. 2002 *Plant Physiology*. Sinauer Associates.

THOMPSON, M. V. & HOLBROOK, N. M. 2003a, Application of a single-solute non-steady-state phloem model to the study of long-distance assimilate transport. *J. Theor. Biol.* **220**, 419–455.

THOMPSON, M. V. & HOLBROOK, N. M. 2003b, Scaling phloem transport: water potential equilibrium and osmoregulatory flow. *Plant, Cell Environ.* **26**, 1561–1577.

WEIR, G. J. 1981 Analysis of Münch theory. *Math. Biosci.* **56**, 141–152.